NANO LETTERS

2008
Vol. 8, No. 8
2463-2468

Multicolor Far-Field Fluorescence Nanoscopy through Isolated Detection of Distinct Molecular Species

Mariano Bossi,[†,‡] Jonas Fölling,[†] Vladimir N. Belov, Vadim P. Boyarskiy, Rebecca Medda, Alexander Egner, Christian Eggeling, Andreas Schönle,* and Stefan W. Hell*

Department of NanoBiophotonics, Max Planck Institute for Biophysical Chemistry, Am Fassberg 11, 37077 Göttingen, Germany

Received May 22, 2008; Revised Manuscript Received July 6, 2008

ABSTRACT

By combining the photoswitching and localization of individual fluorophores with spectroscopy on the single molecule level, we demonstrate simultaneous multicolor imaging with low crosstalk and down to 15 nm spatial resolution using only two detection color channels. The applicability of the method to biological specimens is demonstrated on mammalian cells. The combination of far-field fluorescence nanoscopy with the recording of a single switchable molecular species at a time opens up a new class of functional imaging techniques.

Due to its versatility and ease of use, fluorescence far-field microscopy is one of the most widely used imaging tools in the life sciences. Not only does tagging with fluorescent markers yield excellent molecular specificity and single-molecule sensitivity but the markers themselves can also report on their chemical or physical microenvironment through their spectroscopic characteristics. Thus, by tagging different molecular species with different types of markers, the spatial and temporal correlation of these species can be elucidated. However, in standard far-field microscopy, features of similar spectroscopic properties cannot be separated at distances smaller than ~200 nm, due to diffraction.[1] This fundamental barrier, common to all standard methods based on the focusing of light, persisted for over a century. Meanwhile, the diffraction barrier has been overcome fundamentally by various approaches.[2] A common element in all of them is to select molecular transitions of the marker between a fluorescent and a nonfluorescent state just for the purpose of confining the origin of fluorescence emission in space.[2,3] At first exploited in stimulated emission depletion (STED) microscopy,[4,5] this strategy has matured; meanwhile it allows routine subdiffraction imaging of (living) biological specimens[6,7] with a resolution down to the macromolecular scale.[8]

The insight that the transitions in the marker are the key to diffraction-unlimited resolution has also led to several other far-field "nanoscopy" methods. In all cases, the switching of the marker between a detectable (fluorescent) and a nondetectable (dark) state is used to sequentially gather local information that would otherwise be blurred by diffraction. STED and a number of related concepts that are all based on reversible saturable/switchable optically linear fluorescent transitions (RESOLFT)[9,10] are commonly applied by switching molecules in ensembles, specifically by turning on and off the bright 'fluorescent' state in narrow spots in the sample using a light intensity distribution featuring local zeros (e.g., a doughnut or lines). The subdiffraction image is obtained by scanning the zeros across the sample.

Fluorescent proteins and organic dyes that can be switched to a bright fluorescent state and back to a dark state have led to an alternative approach to image labeled objects with nanometer scale resolution. This approach is based on switching the molecules individually. Single markers that are initially in the dark state are switched to the bright state so sparsely that they are further apart than the diffraction limit. Hence their signals of fluorescence emission are well separated on a camera. Their position can be determined with subdiffraction precision if enough photons are collected from the marker in a burst.[11–16] When this process is repeated multiple times, the sample is stochastically scanned and, consequently, an image can be reconstructed mathematically as a "position histogram" assigning the positions of single emitters to nanosized image regions. Implementations of this stochastic concept have been termed photoactivated localiza-

* To whom correspondence should be addressed. E-mail: aschoen@gwdg.de (A.S.); hell@4pi.de (S.W.H.). Phone: +49 551 201 2500. Fax: +49 551 201 2505.

† These authors contributed equally to this work.

‡ Present address: INQUIMAE-DQIAyQF, Facultad de Ciencias Exactas y Naturales, Universidad de Buenos Aires, Pabellón 2, Ciudad Universitaria, 1428 Buenos Aires, Argentina.

10.1021/nl801471d CCC: $40.75
Published on Web 07/22/2008

tion microscopy (PALM),[17] stochastic optical reconstruction microscopy (STORM),[18] fluorescence PALM (fPALM),[19] and PALM with independently running acquisition (PALM-IRA).[20,21]

We have recently reported a new family of switchable rhodamine dyes whose fluorescence ability can be selectively switched on in a single layer of the sample by two-photon absorption, thus conferring noninvasive optical sectioning to single-molecule-switching-based nanoscopy.[22] In combination with localization along the third dimension, 3D nanoscopy of extended sample regions is feasible,[23,24] thus complementing 3D-approaches based on STED.[25–28]

Fortunately, switching emitters to reach nanoscopical resolution largely maintains the versatility of the fluorescence readout. Consequentially, multicolor STED,[29] PALMIRA,[30] STORM,[31] and PALM[32] have recently been demonstrated. However, in all these cases, the separation of the signal was achieved by using a strategy known from conventional fluorescence microscopy: Markers with distinct activation or excitation spectra were imaged sequentially by choosing the appropriate illumination wavelengths, and the crosstalk between the different color channels was minimized by a careful selection of emission filters. Such a strategy increases the requirements on the spectroscopic properties of the dyes and on the light sources used for excitation and switching and thus increases the complexity of the experiment. Further, sequential imaging compromises the registration accuracy between channels due to sample movement or drifts and results in slower image acquisition.

Importantly, the separate detection of individual molecules offers the possibility to assign every single molecule event to the corresponding dye class, based on a dye-specific property such as the emission spectrum, brightness, lifetime, or anisotropy.[33–37] The key here is to avoid ensemble averaging by ensuring that molecules of different species are never detected simultaneously, which is usually accomplished by using very low concentrations or by mechanical confinement. Likewise, in ensemble-based far-field fluorescence nanoscopy schemes like STED microscopy, the creation of ever smaller focal spots automatically leads to fewer molecules in the focus and thus to the detection of single molecules or individual agglomerates of identical molecules, even if they are densely packed in space. Still, the stochastic imaging methods outlined above are inherently based on the detection of single well separated molecules and therefore directly lend themselves to exploiting the spectroscopic opportunities brought about by detection of a single molecular species at a time. Fluorescence nanoscopy based on switching and computational localization of individual emitters naturally offers the distinction of multiple labels based on their spectroscopic information, even without the need for very distinct spectral properties.[38]

Therefore, in this paper, we depart from the sequential multicolor separation approach and present simultaneous single-molecule-switching-based nanoscale imaging of structures labeled with up to three different switchable rhodamine amides that allow signal separation based on their individual and characteristic emission spectra. Importantly, because we

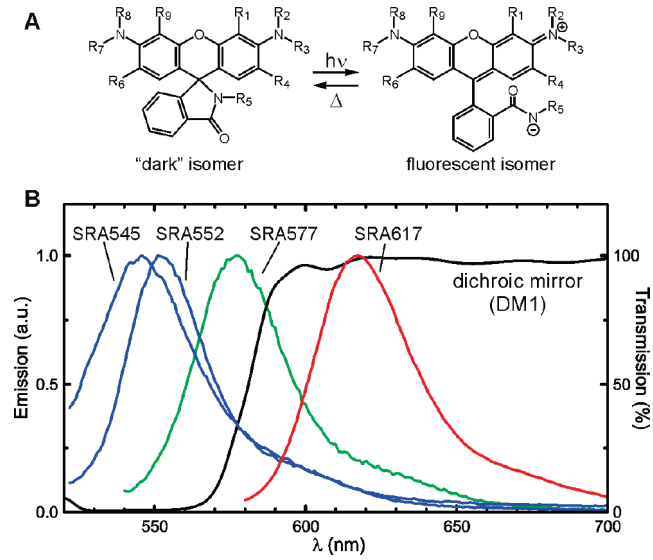

Figure 1. (A) The photochromic switching between bright and dark states of the rhodamine amides used in our experiments. In thermal equilibrium most molecules are in their dark isomeric state. Transition to the fluorescent isomer can be effected by irradiation with UV light. (B) Emission spectra of the fluorescent isomers of SRA545, SRA552, SRA577, and SRA617 in PVA (see Supporting Information). The black line depicts the transmission properties of the dichroic mirror DM1 which we used to split the signal into the two detection channels.

combine spectrally sensitive fluorescence detection with the registration of single switching events, we are able to distinguish $i = 3$ marker types with minimal crosstalk by using just $j = 2$ detection channels. Since it is only limited by the spectral diffusion of single molecules, our approach can be generalized to a constellation in which the number of fluorophore species i exceeds the number of characterizing detection channels j much more significantly.

For each of the experiments reported herein, we have selected up to three of four novel switchable rhodamine amides, denoted SRA545, SRA552, SRA577, and SRA617 according to their emission maximum in poly(vinyl alcohol) (PVA) (Figure 1). Each one is derived from a different stable rhodamine dye (Supplementary Scheme S1). All four compounds can be switched from a dark isomer to a fluorescent one by irradiating them with UV light, which induces a ring-opening reaction of the five-member cycle containing the amide functional group and the spirocarbon atom.[22,39,40] Importantly, these novel markers have the spectroscopic properties required for effective single-molecule-switching-based nanoscopy:[22] (i) The fluorescent isomer is bright and highly stable; thus a large number of photons per event can be detected. This results in high localization accuracy and little crosstalk in multicolor imaging. (ii) Virtually infinite signal contrast between the two states: the dark isomers emit no detectable signal when illuminated at the excitation wavelengths. This eliminates background from the switched-off marker molecules. (iii) The fraction of molecules present in the emitting isomer in a thermally equilibrated sample is very low ($\leq 1{:}10^4$ in all four cases) allowing us to accurately image even densely stained samples. Even there, the activa-

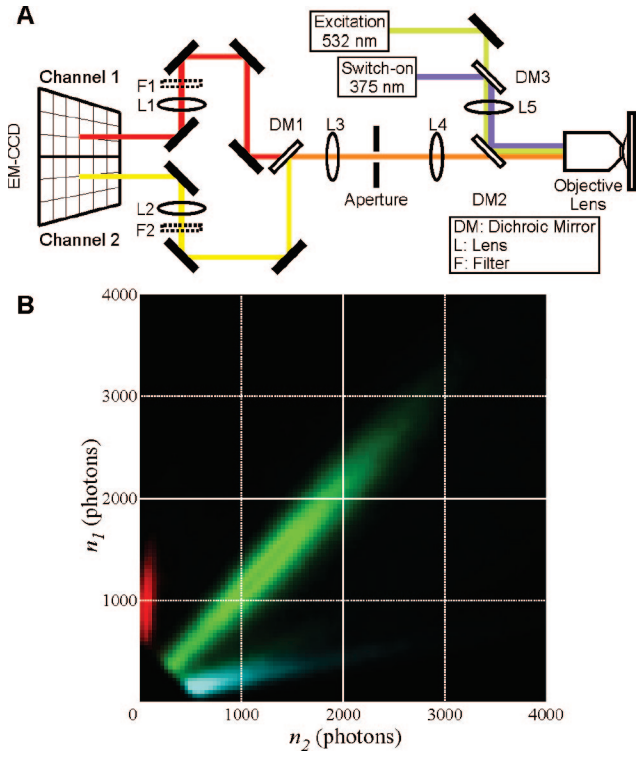

Figure 2. (A) Schematic representation of the two-channel microscope for single-molecule-switching-based multicolor nanoscopy. The sample is illuminated with two lasers at 375 and 532 nm, respectively, combined into one beam by dichroic mirror DM3 and focused by lens L5 into the back-aperture of the objective lens thus providing wide-field illumination (~12 μm in diameter). The fluorescence emitted from isolated switched-on markers is separated from excitation and activation light by dichroic mirror DM2 and then passes the tube lens L4 and a rectangular aperture in the back-focal plane. Using the dichroic mirror DM1, fluorescence is split according to wavelength and directed into two beam paths which image the rectangular aperture onto two adjacent areas on the EM-CCD detector using lenses L3 and L1 or L2. Band-pass filters F1 and F2 were used to minimize out-of-band background. (B) Two-dimensional frequency histogram of the number of detected fluorescence photons n_1 and n_2 from switching events of compounds SRA545 (blue), SRA577 (green), and SRA617 (red) in channels 1 and 2, respectively (number of switching events 32000 (SRA545), 200000 (SRA577), and 14000 (SRA617) extracted from 10240 CCD frames at an excitation intensity of 32 kW/cm^2; events with less than 600 detected photons were rejected).

tion can be tuned such that switching events that are too close to be separated are rare.

The imaging was performed with a simple optical setup resembling a two-color video microscope (Figure 2A). Because no sequential illumination or photoswitching was necessary, the use of two laser wavelengths was sufficient. All markers were switched on with UV light at 375 nm and excited at 532 nm. The signal emitted by the markers was split into two beam paths by a dichroic mirror (DM1, Figure 2A) and each of the channels formed an image on an EM-CCD detector (IXON-Plus DU-860, Andor Technology, Belfast, Northern Ireland): channel 1 containing the light with longer wavelengths and channel 2 containing the light with shorter wavelengths. Additional bandpass filters were used to minimize out-of-band background. The use of an EM-CCD camera at high gain ensured that read-out noise was negligible and that the frame rate of the camera could be optimized to minimize the background.[20,21]

A switching event, i.e., a marker temporarily transferred to its on-state, results in a bright isolated spot in one or several images taken by the CCD camera. In an initial step, such individual events were detected separately in each of the two detection channels, but in the final image reconstruction, it was ensured that events registered in both channels were counted only once. Consequently, for each actual event, we recorded its center of mass and the number of effective photons detected in channel 1, n_1 and in channel 2, n_2 (for the exact definition of n_i see Supporting Information). A marker type can be assigned to each event based on the characteristic ratio n_1/n_2 between the two detection channels. This is detailed in Figure 2B which shows two-dimensional frequency histograms of photon pairs (n_1, n_2) detected for a multitude of single-molecule events of the markers SRA545, SRA577, and SRA617.

Each histogram was obtained by recording subsequent CCD images at sparse activation of a thin Mowiol film with just one of the compounds embedded. Clearly the events from each marker species form a cloud along the line defined by its characteristic ratio. While the length of these clouds is determined by the dye's brightness, their width is dictated by shot and excess noise and the degree of inhomogeneous broadening of the fluorophore's emission spectrum. The dichroic mirror was chosen such as to minimize the overlap of these clouds and thus to split the spectrum of SRA577 approximately in half. Because the type of dye is already known in these experiments, Figure 2B can be seen as a calibration measurement. Properly normalized, it reflects the probability of a dye of a given type to produce a switching event with given intensities n_1 and n_2.

Conversely, when imaging a sample containing all SRA545, SRA577, and SRA617, a detected event (n_1, n_2) can be assigned to the dye which has the highest probability to produce this intensity combination. For this maximum-likelihood estimator, which we used for all our assignments, the probability of erroneously assigning events from one dye type to another one, the crosstalk, is readily estimated from the same calibration measurement as detailed in the Supporting Information. Interestingly, by rejecting events with intensity combinations common for two of the dye types, crosstalk can be minimized at the expense of dynamic range in the image (Supplementary Figure S1).

The probability distribution for each dye may vary with its environment due to variations in the spectrum or quantum yield and thus fluorescence brightness. As an example, one may compare the measurement in Mowiol from Figure 2B with the one in silica beads (Supplementary Figure S1). Most prominently, SRA577 is quenched and its spectrum is shifted to longer wavelengths resulting in a much broader and shorter two-dimensional photon pair frequency histogram. This underscores the importance of a proper calibration measurement for each sample. It should be noted, however, that ensemble multicolor measurements are also affected by spectral shifts and require proper calibration. Even worse,

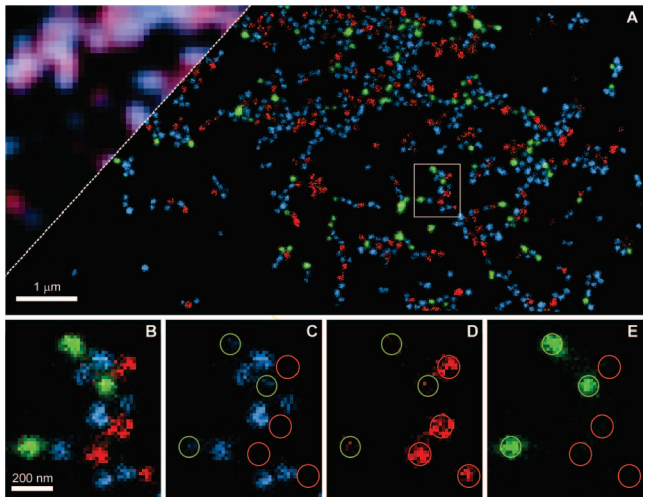

Figure 3. Multicolor single-molecule-switching-based nanoscopy image of mixtures of silica beads each stained with one of three different photoswitchable markers, SRA545 (blue), SRA577 (green), and SRA617 (red). (A) Overview. The upper left triangle shows the image obtained from classical diffraction-limited two-color imaging. No details can be discerned. (B) Enlarged section marked by the white rectangle in the overview and (C−E) blue, red, and green components thereof. Beads identified as green and red are marked, to indicate where crosstalk occurs.

when averaging over many emitters, a change in individual brightness or broadening of the spectrum may be hidden in the ensemble. Using the information on the single-molecule level, we can not only eliminate such bias but also simplify multicolor imaging significantly, since two detection channels proved sufficient for three types of markers. Under favorable conditions the number of marker types can exceed the number of channels even further; separating four or even five markers may be feasible with just two detection channels (Supporting Information).

In order to demonstrate jointly improved resolution and multicolor separation, we imaged samples of multicolored silica nanobeads. To this end, the markers were incorporated in a silica core ~70−90 nm in diameter with a ~15−20 nm wide unlabeled shell grown on top.[41] This preparation ensured a separation of 30−40 nm between the fluorescent cores. The actual sample was prepared by spreading the beads in solution onto a cover glass and letting the ethanol solvent evaporate. Figure 3 shows the image of a mixture of three kinds of beads, each containing one marker type SRA545, SRA577, or SRA617, obtained using our single-molecule-switching-based multicolor nanoscopy approach. Besides the expected nanoscale resolution, our results illustrate the excellent color separation achieved by the method. In contrast to the conventional diffraction-limited wide-field image, our image approach is able to clearly resolve each individual bead and to allocate it to one of the three markers. The image shown was recorded by localizing the switching events in ~75000 EM-CCD frames at a frame acquisition rate of 100 Hz, i.e., a total acquisition time of <13 min. No drift compensation was needed. At an illumination intensity of 32 kW/cm^2, the average number of photons per single molecule burst in a frame ($n_{Ph} = n_1 + n_2$) was 1400 for SRA617, 2100 for SRA577, and 2900 for SRA545, resulting in average localization accuracies (Δx) of 11, 9, and 8 nm, respectively. All events with $n_{Ph} < 600$ were rejected. The localization accuracies were calculated according to $\Delta x = \text{fwhm}/(n_{Ph}/2)^{1/2}$ where fwhm is the classical wide field resolution (~270 nm for our microscope). This estimation for Δx neglects noise arising from background light and camera readout. Note that the division by 2 in the denominator is due to the excess noise of the EM-CCD camera (see Supporting Information for details).[14]

In the first ~30000 frames, the spontaneous switching of the markers was sufficient to ensure a reasonable number of well enough isolated single spots per image frame. Later on, switching-on (activation) light of 440 W/cm^2 was applied in pulses between frames, gradually increasing from 0.1 to 50 μs during the course of the measurement. Figure 3B shows a zoomed area of the nanoscale image, which depicts a few of the differently colored and well-separated beads. Each color component is shown in panels C−E of Figure 3, respectively, along with the marked positions of the other, differently colored beads. The beads labeled with SRA617 have a more spotty appearance because they were loaded with a lower number of markers than those labeled with SRA577 and SRA545. We performed the color allocation according to the outlined procedure, using the appropriate color calibration (Supplementary Figure S1B). As mentioned above, the probability of false color assignation of a marker, that is, the crosstalk, can be tuned in our multicolor nanoscopic imaging approach by rejecting certain events. At the parameters chosen here, the expected values from our calibration measurement are ~6% SRA545 → SRA577 (SRA577 markers falsely recognized as SRA545 ones), ~7% SRA617 → SRA577, ~4% SRA577 → SRA545, ~11% for SRA577 → SRA617 and it was negligible between SRA545 and SRA617. Because beads could be assigned to one of the markers with almost total certainty, we were also able to calculate the actual crosstalk in the image which amounted to 8% SRA545 → SRA577, 5% SRA617 → SRA577, 8% SRA577 → SRA545, and 23% for SRA577 → SRA617.

Besides the sensitivity on the applied environment, one has to observe potential light-induced spectral drifts and inhomogeneous broadening. For example, the emission spectrum of SRA617 slightly shifts to the blue with prolonged irradiation (especially by the UV laser) causing its distribution to increasingly overlap with that of SRA577. The same effect was observed for SRA577, but to a lesser extent. Thus the ideal calibration would have to change during the course of a measurement; its omission results in additional crosstalk. Here, we have simply elected to measure for only 75000 frames. As expected, the SRA577 → SRA617 crosstalk was elevated due to the shift; however, the light dose was low enough for the time-independent calibration to be still acceptable. For longer measurement times more sophisticated calibration methods must be employed.

We also recorded nanoscopic images of two-color labeled cellular samples. To this end, the microtubule and keratin network of mammalian cells were immunostained following a previously described protocol,[22] with secondary antibodies labeled with SRA577-NHSS and SRA552-maleimide, re-

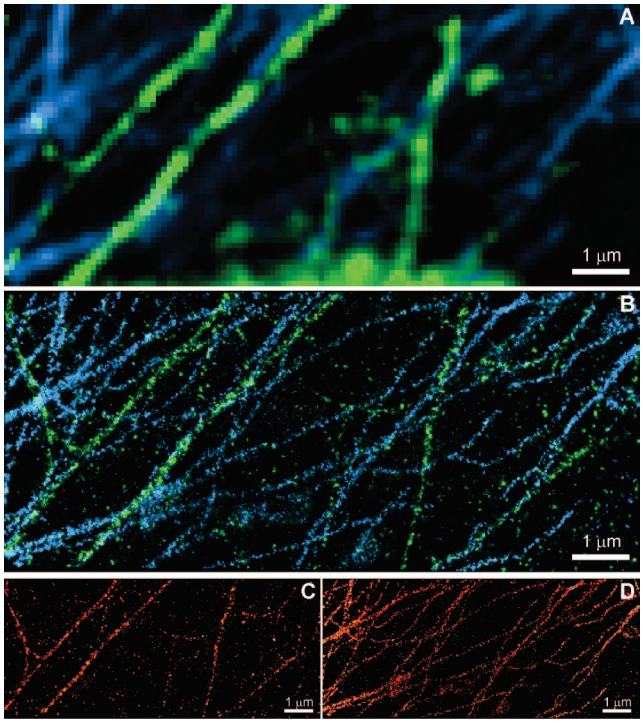

Figure 4. Multicolor single-molecule-switching-based nanoscopy image of an intact mammalian PtK2 cell, the microtubule and keratin network immunostained with the two rhodamine amides SRA552-maleimide (blue) and SRA577-NHSS (green), respectively. (A) Classical wide-field image, linearly unmixed. (B) Nanoscopy image. (C) Microtubule network (blue component in B). (D) Keratin network (green component in B).

spectively. SRA552 replaced SRA545 due to the much better solubility in water (facilitating immunolabeling). Images of this doubly labeled cellular sample are shown in Figure 4. The frame rate for image acquisition was 200 Hz at a total number of 90000 frames, resulting in a total acquisition time of 7.5 min (due to the increase in brightness compared to the bead measurement, the integration time was lowered—compare Supplementary Figures S1 and S2). All events with less than 400 photons in total were rejected. At an excitation intensity of 19 kW/cm^2 and frame integration time of 5 ms, the mean number of effective photons is 2600 for SRA552 and 1200 for SRA577. The first 10000 frames were recorded with no activation light, and then pulses of 440 W/cm^2 were applied with exposure lengths increasing from 1 μs to 1 ms (pulses longer than 50 μs, the camera dark-time between frames, span into the recording of a frame). The crosstalk between the two markers expected from calibration measurements (Supplementary Figure S2) is ~5%. Therefore, both microtubule and keratin filaments are clearly resolved and separated.

Two-color separation is also possible in the counterpart wide-field images (Figure 4A) because the number of channels is equal to the number of marker types, making linear unmixing processes applicable. In fact, linear unmixing was mandatory due to the crosstalk of ~30% resulting from the emission spectra of the dyes (see Figure 1B). While this process improves the color separation, it inevitably also elevates the noise of the image. We did not use linear unmixing in any of the nanoscopy recordings obtained with the single molecule spectroscopy approach. However, unlike in conventional wide-field microscopy, linear unmixing is possible even when the number of marker types i exceeds the number of detection channels j.

Besides the filament structures, we also observed single isolated spots (predominantly in the SRA577 channel of the super-resolved image). These additional grainy features seem to be common in single-molecule-switching-based nanoscopy (see for example refs 22, 23, and 30−32). Here, we attribute these spots to unspecific binding of the primary antibodies.

We have thus presented nanoscale colocalization of multiply labeled molecules or cellular structures by using slight spectral differences in the emission characteristics of the different fluorescent markers. At spatial resolutions of ~10−15 nm, this technique, along with multicolor STED, will close the gap between Förster resonance energy transfer (FRET) and classical microscopy in colocalization experiments. While FRET imaging probes the efficiency of energy transfer between two dyes at a distance of 1−10 nm,[42] classical colocalization is limited to distances >200 nm given by diffraction. Our photoswitchable rhodamine amides provide a large number of photons per detected molecule, and thus high localization accuracy (up to 8 nm) in the imaging plane. They are based on chemical modifications of the base rhodamine chromophore[43] which can be applied to other rhodamines to create additional markers in the future. Combined with the ability to photoswitch their fluorescence by two-photon absorption for optical sectioning, these dyes are thus a simple alternative to cyanine dye pairs[31] and might be a key ingredient in extending it to the third dimension.

Using the emission spectrum to discern the labels constitutes a methodical advancement over the sequential recording used in earlier multicolor experiments. It brings about the important advantage that only one laser source is used for either switching the markers on or exciting their fluorescence as compared to previous multicolor experiments. On the detection and analysis side, all data are recorded simultaneously, which accelerates the image recording, thereby minimizing sample drifts during acquisition. It also simplifies the alignment of the differently hued images. Likewise, crosstalk was much lower than that in the ensemble measurements, completely eliminating the need for linear unmixing. With the right choice of dyes and dichroic mirror, the number of markers i discernible by two detection channels should be extendable.

The underlying reason for this fact is that by measuring single molecules at a time, we inherently measure only a single molecular species. It is important to note that the strategy described herein is not strictly limited to single molecule detection. The requirement ultimately is that only a single molecular species is recorded at a time. Imagine, for example, an ensemble-based fluorescence nanoscopy approach such as STED microscopy featuring a nanosized focal spot, for example, of the size of an antibody. Assume that the object is labeled with antibodies of different colors, whereby each antibody is conjugated to several molecules. If only one type of colored antibody is in the focal spot at a

given point in time (which becomes increasingly more likely with smaller focal spots), our procedure can be applied just as effectively. Hence, although it is most naturally implemented with single-molecule-based approaches, our method is not restricted to single molecule nanoscopy schemes. This insight is important, because the probability of identifying only a single species or a spectrally homogeneous feature at a time naturally increases with increasing spatial resolution.

We also note that besides the emission wavelength, other parameters such as fluorescence lifetime, anisotropy, or FRET efficiency could similarly be exploited. On one hand, they can be used to distinguish even more reliably between different markers. On the other hand, markers that are sensitive to their environment may be used to probe, for example, local pH, temperature, rotational mobility, proximity to other markers, and other physical or chemical parameters. Thus, combining spectroscopy and nanoscopy as outlined above should open a whole new field of applications in life science and beyond.

Acknowledgment. The authors are grateful to R. Machinek, H. Frauendorf, and their co-workers at the Institut für Biomolekulare and Organische Chemie (Georg-August-Universität Göttingen) for measuring NMR and mass spectra. We also thank Claas v. Middendorf and Claudia Geisler for insightful discussions, Daniel Neumann for help with the biological samples, and Jaydev Jethwa for critical reading of the manuscript. This work was supported by the European Commission through a Marie Curie Fellowship (to M.B.) and by a network grant (SPOTLITE) within the program on New and Emerging Science and Technology (NEST) (to S.W.H.); further support is acknowledged from the German Ministry of Education and Research (BMBF) through the Biophotonics III program.

Supporting Information Available: Figures detailing the calibration measurements and the resulting identification matrices used to create Figures 2 and 3 and containing additional information on the spectroscopy of the dyes in use, a discussion on camera noise, localization accuracy and fundamental limitations of the approach, and details on the estimation and comparison of crosstalk for ensemble and single-species detection, and chemical structure of the dyes and a detailed description of the setup and the techniques used for the preparation of the mammalian cells. This material is available free of charge via the Internet at http://pubs.acs.org.

References

(1) Abbe, E. *Arch. Mikrosk. Anat.* **1873**, *9*, 413–468.
(2) Hell, S. W. *Science* **2007**, *316* (5828), 1153–1158.
(3) Hell, S. W. *Opt. Commun.* **1994**, *106*, 19–24.
(4) Hell, S. W.; Wichmann, J. *Opt. Lett.* **1994**, *19* (11), 780–782.
(5) Klar, T. A.; Jakobs, S.; Dyba, M.; Egner, A.; Hell, S. W. *Proc. Nat. Acad. Sci. U.S.A.* **2000**, *97*, 8206–8210.
(6) Willig, K. I.; Rizzoli, S. O.; Westphal, V.; Jahn, R.; Hell, S. W. *Nature* **2006**, *440* (7086), 935–939.
(7) Westphal, V.; Rizzoli, S. O.; Lauterbach, M. A.; Kamin, D.; Jahn, R.; Hell, S. W. *Science* **2008**, *320* (5873), 246–249.
(8) Donnert, G.; Keller, J.; Medda, R.; Andrei, M. A.; Rizzoli, S. O.; Lührmann, R.; Jahn, R.; Eggeling, C.; Hell, S. W. *Proc. Natl. Acad. Sci. U.S.A.* **2006**, *103* (31), 11440–11445.
(9) Hell, S. W. *Phys. Lett. A* **2004**, *326* (1−2), 140–145.
(10) Hofmann, M.; Eggeling, C.; Jakobs, S.; Hell, S. W. *Proc. Natl. Acad. Sci. U.S.A.* **2005**, *102* (49), 17565–17569.
(11) Bobroff, N. *Rev. Sci. Instrum.* **1986**, *57* (6), 1152–1157.
(12) Betzig, E. *Opt. Lett.* **1995**, *20* (3), 237–239.
(13) Hell, S. W.; Soukka, J.; Hänninen, P. E. *Bioimaging* **1995**, *3*, 65–69.
(14) Schmidt, T.; Schutz, G. J.; Baumgartner, W.; Gruber, H. J.; Schindler, H. *Proc. Natl. Acad. Sci. U.S.A.* **1996**, *93* (7), 2926–9.
(15) Lacoste, T. D.; Michalet, X.; Pinaud, F.; Chemla, D. S.; Alivisatos, A. P.; Weiss, S. *Proc. Natl. Acad. Sci. U.S.A.* **2000**, *97* (17), 9461–9466.
(16) Thompson, R. E.; Larson, D. R.; Webb, W. W *Biophys. J.* **2002**, *82*, 2775–2783.
(17) Betzig, E.; Patterson, G. H.; Sougrat, R.; Lindwasser, O. W.; Olenych, S.; Bonifacino, J. S.; Davidson, M. W.; Lippincott-Schwartz, J.; Hess, H. F. *Science* **2006**, *313* (5793), 1642–1645.
(18) Rust, M. J.; Bates, M.; Zhuang, X. *Nat. Methods* **2006**, *3*, 793–796.
(19) Hess, S. T.; Girirajan, T. P. K.; Mason, M. D *Biophys. J.* **2006**, *91* (11), 4258–4272.
(20) Geisler, C.; Schönle, A.; von Middendorff, C.; Bock, H.; Eggeling, C.; Egner, A.; Hell, S. W. *Appl. Phys. A: Mater. Sci. Process.* **2007**, *88* (2), 223–226.
(21) Egner, A.; Geisler, C.; von Middendorff, C.; Bock, H.; Wenzel, D.; Medda, R.; Andresen, M.; Stiel, A.-C.; Jakobs, S.; Eggeling, C.; Schönle, A.; Hell, S. W *Biophys. J.* **2007**, *93*, 3285–3290.
(22) Fölling, J.; Belov, V.; Kunetsky, R.; Medda, R.; Schönle, A.; Egner, A.; Eggeling, C.; Bossi, M.; Hell, S. W. *Angew. Chem., Int. Ed.* **2007**, *46*, 6266–6270.
(23) Huang, B.; Wang, W.; Bates, M.; Zhuang, X. *Science* **2008**, *319*, 810–813.
(24) Juette, M. F.; Gould, T. J.; Lessard, M. D.; Mlodzianoski, M. J.; Nagpure, B. S.; Bennett, B. T.; Hess, S. T.; Bewersdorf, J. *Nat. Methods* **2008**, *5*, 527–529.
(25) Dyba, M.; Hell, S. W. *Phys. Rev. Lett.* **2002**, *88*, 163901.
(26) Dyba, M.; Jakobs, S.; Hell, S. W. *Nat. Biotechnol.* **2003**, *21* (11), 1303–1304.
(27) Harke, B.; Ullal, J.; Keller, J.; Hell, S. W. *Nano Lett.* **2008**, *8* (5), 1309–1313.
(28) Schmidt, R.; Wurm, C. A.; Jakobs, S.; Engelhardt, J.; Egner, A.; Hell, S. W *Nat. Methods* **2008**, *5*, 539–544.
(29) Donnert, G.; Keller, J.; Wurm, C. A.; Rizzoli, S. O.; Westphal, V.; Schönle, A.; Jahn, R.; Jakobs, S.; Eggeling, C.; Hell, S. W. *Biophys. J.* **2007**, *92* (8), L67–69L.
(30) Bock, H.; Geisler, C.; Wurm, C. A.; Jakobs, S.; Schönle, A.; Egner, A.; Hell, S. W.; Eggeling, C *Appl. Phys. B: Laser Opt.* **2007**, *88*, 161–165.
(31) Bates, M.; Huang, B.; Dempsey, G. P.; Zhuang, X. *Science* **2007**, *317*, 1749–1753.
(32) Shroff, H.; Galbraith, C. G.; Galbraith, J. A.; White, H.; Gillette, J.; Olenych, S.; Davidson, M. W.; Betzig, E. *Proc. Natl. Acad. Sci. U.S.A.* **2007**, *104* (51), 20308–20313.
(33) Shera, E. B.; Seitzinger, N. K.; Davis, L. M.; Keller, R. A.; Soper, S. A. *Chem. Phys. Lett.* **1990**, *174* (6), 553–557.
(34) Zander, C.; Sauer, M.; Drexhage, K. H.; Ko, D.-S.; Schulz, A.; Wolfrum, J.; Brand, L.; Eggeling, C.; Seidel, C. A. M. *Appl. Phys. B: Laser Opt.* **1996**, *63*, 517–523.
(35) Ha, T.; Enderle, T.; Chemla, D. S.; Selvin, P. R.; Weiss, S. *Phys. Rev. Lett.* **1996**, *77* (19), 3979–3982.
(36) Ha, T.; Enderle, T.; Chemla, D. S.; Weiss, S. *IEEE J. Sel. Top. Quantum Electron.* **1996**, *2* (4), 1115–1128.
(37) Fries, J. R.; Brand, L.; Eggeling, C.; Köllner, M.; Seidel, C. A. M. *J. Phys. Chem. A* **1998**, *102*, 6601–6613.
(38) Schönle, A.; Hell, S. W. *Nat. Biotechnol.* **2007**, *25* (11), 1234–1235.
(39) Knauer, K. H.; Gleiter, R. *Angew. Chem., Int. Ed.* **1977**, *16* (2), 113–113.
(40) Willwohl, H.; Wolfrum, J.; Gleiter, R. *Laser Chem.* **1989**, *10*, 63–72.
(41) Fölling, J.; Belov, V.; Riedel, D.; Schönle, A.; Egner, A.; Eggeling, C.; Bossi, M.; Hell, S. W. *ChemPhysChem* **2008**, *9*, 321–326.
(42) Jares-Erijman, E. A.; Jovin, T. M. *Nat. Biotechnol.* **2003**, *21* (11), 1387–1395.
(43) Boyarskiy, V. P.; Belov, V. N.; Medda, R.; Hein, B.; Bossi, M.; Hell, S. W. *Chem.-Eur. J.* **2008**, *14*, 1784–1792.

NL801471D